Published in final edited form as:
Neurotoxicology. 2013 December ; 0: . doi:10.1016/j.neuro.2013.09.001.

Bortezomib alters microtubule polymerization and axonal transport in rat dorsal root ganglion neurons

Nathan P. Staff[1,*], **Jewel L. Podratz**[1], **Lukas Grassner**[1,4], **Miranda Bader**[1], **Justin Paz**[1], **Andrew M. Knight**[1], **Charles L. Loprinzi**[2], **Eugenia Trushina**[1,3], and **Anthony J. Windebank**[1]

[1]Department of Neurology, Mayo Clinic College of Medicine, Mayo Clinic, Rochester, MN USA

[2]Department of Oncology, Mayo Clinic College of Medicine, Mayo Clinic, Rochester, MN USA

[3]Department of Molecular Pharmacology and Experimental Therapeutics, Mayo Clinic College of Medicine, Mayo Clinic, Rochester, MN USA

Abstract

Bortezomib is part of a newer class of chemotherapeutic agents whose mechanism of action is inhibition of the proteasome-ubiquitination system. Primarily used in multiple myeloma, bortezomib causes a sensory-predominant axonal peripheral neuropathy in approximately 30% of patients. There are no established useful preventative agents for bortezomib-induced peripheral neuropathy (BIPN), and the molecular mechanisms of BIPN are unknown. We have developed an *in vitro* model of BIPN using rat dorsal root ganglia neuronal cultures. At clinically–relevant dosages, bortezomib produces a sensory axonopathy as evidenced by whole explant outgrowth and cell survival assays. This sensory axonopathy is associated with alterations in tubulin and results in accumulation of somatic tubulin without changes in microtubule ultrastructure. Furthermore, we observed an increased proportion of polymerized tubulin, but not total or acetylated tubulin, in bortezomib-treated DRG neurons. Similar findings are observed with lactacystin, an unrelated proteasome-inhibitor, which argues for a class effect of proteasome inhibition on dorsal root ganglion neurons. Finally, there is a change in axonal transport of mitochondria induced by bortezomib in a time-dependent fashion. In summary, we have developed an *in vitro* model of BIPN that recapitulates the clinical sensory axonopathy; this model demonstrates that bortezomib induces an alteration in microtubules and axonal transport. This robust model will be used in future mechanistic studies of BIPN and its prevention.

Keywords

bortezomib; chemotherapy-induced peripheral neuropathy; peripheral neuropathy; neurotoxicity; dorsal root ganglia; rat

[*]Corresponding Author: Nathan P. Staff, M.D., Ph.D., Mayo Clinic College of Medicine, 200 First Street SW, Rochester, MN 55905 USA. staff.nathan@mayo.edu.

[4]Current address for Lukas Grassner: Spinal Cord Injury and Tissue Regeneration Center, Institute for Molecular Regenerative Medicine, Paracelsus Medical University Salzburg, Austria

1. Introduction

Chemotherapy-induced peripheral neuropathy (CIPN) is a serious side-effect that often limits chemotherapy dosage. Pain and other quality of life impairments caused by CIPN are on the rise, as many forms of cancer become chronic conditions. Protective strategies are complicated by the possibility that preventing CIPN may reduce the primary cancer cell killing effect of a drug.

Bortezomib (Velcade®) is the first member of a new class of chemotherapeutic agents that inhibit the proteasome-ubiquitination pathway, a critical pathway for intracellular protein degradation (Adams et al., 1998). It does this by reversible binding and inhibition of the 26S subunit of the proteasome. Bortezomib is FDA-approved for use in multiple myeloma and mantle cell lymphoma, and is being investigated for use in a host of other hematological and solid tumors.

Bortezomib causes a painful axonal sensory-predominant length-dependent peripheral neuropathy in 30–40% of patients that limits the allowable dosage (Barr et al., 2009, Mauermann et al., 2012, Richardson et al., 2006). Bortezomib-induced peripheral neuropathy (BIPN) may be seen in patients with or without pre-existing peripheral neuropathy from their underlying cancer. Interestingly, approximately 2/3 of patients with BIPN have improvement or resolution of neuropathic symptoms following bortezomib discontinuation (Richardson, Briemberg, 2006). The combination of length-dependent phenotype, clinical neurophysiology that predicts axonal pathology, and clinical reversibility suggests that minimal neuronal death is occurring and that the primary pathophysiology is of a “dying back” toxic axonal neuropathy (Boyette-Davis et al., 2011).

Several mechanisms of action for bortezomib-induced cancer cell death have been proposed. The most prominent theory for its cancer-killing properties is the decreased activation of nuclear factor kappa-light-chain-enhancer of activated B cells (NF-ΚB) that leads to apoptosis (Traenckner et al., 1994a). It has been demonstrated that in the presence of bortezomib, the inhibitory factor for NF-ΚB (IF-ΚB) is not degraded properly via the proteasome pathway and is thus available for continued inhibition of NF-ΚB (Traenckner et al., 1994b). Other mechanisms of action for cancer cell death have been established, including effects on the Bcl-2 family members, constitutive activation of c-Jun N-terminal kinase (JNK), upregulation of p53, and increased endoplasmic reticulum stress (Voorhees and Orlowski, 2006). The relation of these cancer cell death mechanisms to BIPN has not been established.

The mechanisms of BIPN are unclear. In order to begin to mechanistically understand BIPN, we now describe an *in vitro* model of bortezomib-induced peripheral neuropathy utilizing the cell type that is affected in this condition, the dorsal root ganglion sensory neurons.

2. Materials and Methods

Dorsal root ganglia (DRG) from embryonic day 15 Sprague-Dawley rat were used for all experiments in this study, as approved by the Mayo Clinic Institutional Animal Care and Use Committee. Rat DRG cultures are an established model to study various mechanisms of neurotoxicity (Gill and Windebank, 1998, Podratz et al., 2011, Scuteri et al., 2006, Ta et al., 2006, Windebank et al., 1994).

2.1 DRG Explant Neurite Outgrowth Model

Whole DRG were harvested and plated on collagen-coated plastic dishes and incubated in enhanced minimally-enriched media (EMEM) AN2 medium containing 10% calf bovine

serum (Hyclone, Logan, UT), 7 mg/ml glucose (Sigma, St. Louis, MO) 1.2 mM L-glutamine (Invitrogen, Carlsbad, CA) and 10 ng/ml NGF (Bioproducts for Sciences, Indianapolis, IN). The incubation media contained varying concentrations of bortezomib (LC Laboratories, Woburn, MA) or lactacystin (Peptides International, Louisville, KY). Phase contrast low power micrographs were obtained at 24 and 48 hours after culture. Measurements were made from the edge of the DRG radially to the end of the longest neurite outgrowth using Image J software (NIH).

2.2 Cell Culture Model

DRG were mechanically dissociated aided by trypsin digestion (0.25%) and plated on poly-lysine coated plastic dishes incubated with AN2 as previously described with 15% calf bovine serum (Ta, Espeset, 2006). Cultures were treated with 20 μM 2, 5 fluoro-2-deoxyuridine (Sigma, St. Louis, MO) and 20 μM uridine (Sigma, St. Louis, MO) for 3–5 days to decrease the numbers of supporting cells, after which neuron-enriched cultures were treated with drug and processed as outlined below.

DRG neurons were treated with bortezomib (50, 100, or 200 nM) for 48 hours; cells from the same plating without bortezomib treatment were used as control. Cell survival was estimated using direct cell counting, and apoptosis was detected using morphological observation of nuclear fragmentation. For cell survival, dissociated DRG neurons were plated on plastic tissue culture dishes etched with a grid. The grids were marked and neurons for the same group were counted manually using Image J software at 0, 24, and 48 hours. DRG cultures were fixed with 4% paraformaldehyde for 10 minutes, mounted with VECTASHIELD mounting medium (Vector Labs, Burlingame, CA) containing 4', 6-diamidino-2-phenylindole (DAPI), and observed by light microscopy for nuclear fragmentation signifying apoptosis. Phase contrast low power (20× magnification) light micrographs were obtained and manually assessed in a blinded-fashion. Only obvious nuclear fragmentation was counted as an apoptotic event.

2.3 Immunohistochemistry

Dissociated DRG neurons with and without bortezomib (100 nM) or lactacystin (10 μM) treatment were washed with phosphate buffered saline (PBS) and then fixed with 4% paraformaldehyde for 10 minutes. Cells were treated with PBS-Triton-X (0.05%) for five minutes, washed with PBS-Tween (0.1%) and blocked with 20% goat serum in PBS-Tween. Neurons were incubated for one hour at room temperature in 1:200 anti-Tuj-1 monoclonal antibody (Neuromics Antibodies, Edina, MN) to stain for beta-tubulin. Neurons were washed and incubated in 1:400 goat antimouse antibody conjugated to Cy3 (Jackson ImmunoResearch, Baltimore Pike, CO). Neurons were mounted on slides using VECTASHIELD mounting medium with DAPI. Images were obtained using either a Zeiss Axiovert fluorescent microscope (Carl Zeiss Microimaging Inc., Thornwood, NY) or Zeiss LSM 500 laser scanning confocal microscope (Carl Zeiss Microimaging Inc., Thornwood, NY).

To quantify the somatic tubulin staining, low power (20× magnification) epifluorescence micrographs were obtained in control, bortezomib and lactacystin-treated cells at identical fluorescence exposure times. In order to quantify somatic tubulin ring epifluorescence in an unbiased fashion, the pixel intensity threshold was set for selected micrographs to define the somatic ring epifluorescence. This pixel intensity was then subtracted uniformly from all micrographs. This resulted in images where tubulin ringed soma were present without lower level staining in other portions of the cell culture. Micrographs were then randomized and the interpreter was blinded to the culture treatment. Ringed soma were then manually counted and presented as a fraction of all soma.

2.4 Electron Microscopy

Whole DRG explants were cultured as described above, allowing neurite outgrowth for 48 hours. DRG were washed with PBS and fixed for transmission electron microscopy (TEM) in Trump's fixative consisting of 4% formaldehyde, 1% glutaraldehyde in PBS (pH 7.2). Cells were postfixed in 1% osmium tetroxide and stained en bloc with 2% uranyl acetate. DRG were embedded in a mixture of Epon and araldite. All reagents were obtained from Electron Microscope Services (Ft. Washington, PA). Ultrathin sections (100 nm) were cut from the same blocks, mounted on 200 μm mesh copper grids, stained with lead citrate, examined and photographed using an FEI Technai 12 transmission electron microscope at 100 kV (Fei, Inc., Hillsboro, OR), equipped with a digital CCD camera (Advanced Microscopy Techniques, Danvers, MA).

2.5 Western Blot Analysis

DRG were washed with PBS, scraped from the tissue culture dish and homogenized in NP40 Cell Lysis buffer (Invitrogen, Camarillo, CA). Protein was determined using DC Protein assay (Bio-Rad, Hercules, CA). 10 μg of protein was run per lane on a 10–20% PAGE and then transferred onto PVDF membrane. For determination of acetylated tubulin, PVDF membranes were sequentially blotted with antibodies for tubulin (1:10,000; anti-Tuj-1), anti-acetylated tubulin monoclonal antibody (1:10,000; Sigma-Aldrich, St. Louis, MO) and anti-GAPDH monoclonal antibody (1:10,000; Cell Signaling, Boston, MA), stripping the membrane with guanidine (7M) in between blots. Detection of the proteins was carried out using a BM Chemiluminescence Western Blotting kit containing the secondary antibody (Roche, Mannheim, Germany) exposed onto film. Micrographs of exposed films were produced using AlphaImager2200 (ProteinSimple, Santa Clara, CA) and densitometry was performed on Image J software (NIH). This experiment was performed on three litters and tubulin and acetylated tubulin measurements were normalized to GAPDH levels.

Tubulin polymerization was determined using an assay adapted from Poruchynsky et al. (Poruchynsky et al., 2008). In brief, DRG were washed with PBS, and scraped from the tissue culture dish in a hypotonic lysis buffer containing MgCl2 (0.5 mM), EGTA (1 mM), Tris-HCl (10 mM), paclitaxel (5 μM), Trichostatin-A (10 μM), Nonidet P-40 (0.5%) and protease inhibitors (Roche Diagnostics, Mannheim, Germany). Cells were incubated at 37 degrees Celsius for 15 minutes, vortexed vigorously for 20 seconds and then centrifuged for 10 minutes at 15,000 g at room temperature. The supernatant (soluble tubulin) was placed in a separate eppendorf tube and an equal amount of hypotonic lysis buffer was replaced in the eppendorf tube containing the pellet (polymerized tubulin), which was then sonicated to resuspend proteins. 10–20% PAGE gels were loaded with equal volume of protein sample in the soluble and polymerized portions and then transferred onto PVDF membrane that was subsequently blotted with anti-Tuj 1 monoclonal antibody (1:10,000). Quantification of bands was performed as described above and expressed as a fraction of polymerized tubulin to total tubulin (polymerized tubulin / soluble + polymerized tubulin), which was then normalized to control conditions. This experiment was performed on four litters.

2.6 Axonal Transport Studies

DRG neuronal cultures were prepared as described above and subsequently treated with bortezomib (100 nM) for varying duration (6, 12, and 24 hours) prior to mitochondrial labeling. Evaluation of axonal trafficking of mitochondria was done with 10 nM tetramethylrhodamine methyl ester (TMRM) (Molecular Probes, Eugene, Oregon) for 10 minutes as described previously (Trushina et al., 2004). Mitochondria were imaged at 37° Celsius with a LSM 510 confocal microscope (Carl Zeiss Inc., Thornwood, N.Y.) with a Plan-Apochromat 100× (1.4 n.a.) oil objective with the confocal aperture fully opened. Five minute movies (one second per frame) were acquired. Experiments were performed three

times and off-line analysis of mitochondria motility was performed in a blinded and randomized fashion as described previously (Trushina, Dyer, 2004).

2.7 Statistical Analysis

Data was analyzed for means and SEM using one-way analysis of variance (ANOVA) of data with parametric distribution (Gaussian). Statistical significance was analyzed using Tukey-Kramer multiple comparison post-test using Prism software (GraphPad Software, La Jolla, CA).

3. Results

3.1 Bortezomib inhibits DRG neurite outgrowth without causing cell death

Using a whole DRG explant organotypic culture neurite outgrowth assay (Ta, Espeset, 2006) (Figure 1A), we determined that bortezomib causes a dose-dependent inhibition of neurite outgrowth (Figure 1B). At 48 hours in control media the mean DRG neurite outgrowth was 973.1 ± 74.4 μm, which progressively decreased in the presence of 50 nM (731.1 ± 35.0 μm), 100 nM (435.5 ± 111.7 μm), and 200 nM bortezomib (264.5 ±101.1 μm) ($p<0.05$). In a separate set of experiments, lactacystin, a proteasome inhibitor that inhibits the 20S proteasome subunit (bortezomib inhibits the 26S proteasome subunit), caused a similar inhibition of neurite outgrowth (at 48 hours, control 1889.3 ± 68.3 μm, lactacystin 10 μM 764.0 ± 38.1 μm, $p<0.05$, paired t-test). Neurite outgrowth inhibition was not associated with neuronal cell death, as determined in cell survival experiments (dissociated DRG neuronal cultures Figure 1C, D) (Ta, Espeset, 2006). Neurons in DRG cultures treated with control media did not exhibit cell death at 48 hours in the presence of 50 nM (97.3 ± 0.6%), 100 nM (101.7 ± 2.6%) or 200 nM bortezomib (102.4 ±1.8%) ($p > 0.05$). Furthermore, there was no evidence of increased apoptosis in bortezomib-treated cultured DRG neurons up to 72 hours of exposure as assessed by DAPI nuclear fragmentation (0.3 ± 0.1% apoptosis in control media versus 0.5 ± 0.1% apoptosis in 100 nM bortezomib for 72 hours) ($p > 0.05$).

These data support the hypothesis that bortezomib preferentially affects neurites, which mirrors the clinical phenotype of bortezomib-induced peripheral neuropathy in patients, which has features primarily of a “dying-back” axonal sensory neuropathy (Richardson, Briemberg, 2006). For subsequent experiments with dissociated DRG neurons, a 100 nM dose of bortezomib was chosen because of its intermediate effect in neurite outgrowth experiments (45% neurite outgrowth inhibition). Furthermore, in humans, a standard dose of bortezomib (1.3 mg/m^2) yields a median peak blood concentration of 509 ng/mL, with 83% bound to plasma proteins (Bross et al., 2004). Overall, this corresponds to a free concentration of 110 nM bortezomib at peak, similar to the dose employed in these experiments.

3.2 Bortezomib induces somatic aggregation of beta-tubulin without altering microtubule ultrastructure

Based on the initial observations illustrated in Figure 1, we hypothesized that bortezomib mediates its effect on DRG neurite outgrowth via disruption of cytoskeletal architecture, a common cause of acquired and inherited peripheral neuropathy. Immunohistochemistry studies of control dissociated DRG neurons (Figure 2A, 3A) and neurons treated with bortezomib (Figure 2B, 3B–C) or lactacystin (Figure 2D) revealed unique ring-like somatic aggregation of beta-tubulin. The percentage of somata with tubulin aggregation was significantly increased in 100 nM bortezomib- (72 ± 4.2%) and 10 μM lactacystin-treated neurons (51 ± 2.9%) compared to controls (27 ± 5.8%; $p < 0.05$) (Figure 2C).

Using confocal microscopy, tubulin aggregation appeared to localize in a sub-plasma membrane region (Figure 3C). We did not detect this aggregation of polymerized microtubules in transmitted electron microscopy (data not shown). Ultrastructure of formed microtubules appeared normal within DRG neurites exposed to bortezomib, judged by their appearance on the micrographs generated using transmitted electron microscopy (Figure 4 A, B).

3.3 Bortezomib increases fraction of polymerized tubulin in DRG neurons

Proteasome inhibition has been shown to increase microtubule polymerization in other cell culture models (Poruchynsky, Sackett, 2008). We used a Western blot assay that quantifies the fraction of polymerized tubulin in a sample (Poruchynsky, Sackett, 2008). Bortezomib (100 nM) exposure did not affect total amounts of tubulin (ratio of control:bortezomib chemiluminescence = 1:1.04 ± 0.06) (Figure 5B). Alternatively, polymerized tubulin was increased in DRG treated for 24 hours with either 100 nM bortezomib (normalized percentage polymerized tubulin 115% ± 3.4) or 10 μM lactacycstin (normalized percentage polymerized tubulin 122% ± 6.6) ($p<0.05$) (Figure 5A,C). Tubulin polymerization is often associated with increased tubulin acetylation. Increased levels of acetylated tubulin were not observed in DRG treated with either 100 nM bortezomib (normalized acetylated tubulin 0.93 ± 0.10) or 10 μM lactacycstin (normalized acetylated tubulin 0.88 ± 0.24) ($p>0.05$) (Figure 5B, D).

3.3 Bortezomib inhibits mitochondrial axonal transport

Taking into consideration the abnormalities in microtubule polymerization, we hypothesized that axonal transport would be affected as seen in other chemotherapeutic agents that affect microtubules (Lapointe et al., 2013). This was directly tested using a time lapse imaging of mitochondria labeled with TMRM (10 nM) in live DRG neurons (Figure 5A–C) (Trushina, Dyer, 2004). There was a clear time-dependent effect of 100 nM bortezomib on mitochondrial axonal transport. When normalized for the number of mitochondria in a given neurite, there was a progressive decrease in the frequency of mitochondrial movements observed within the five minute-observation with the increase in bortezomib treatment time (baseline: 0.54 ± 0.13, six hours: 0.44 ± 0.09, twelve hours: 0.31 ± 0.05, 24 hours: 0.17 ± 0.02 movements/mitochondria; $p < 0.05$ at 24 hours) (Figure 6D). The average velocity of mitochondrial movement (Figure 6E) decreased with increasing exposure time where there was clear statistical significance within 12 hours (baseline: 1.11 ± 0.03, six hours: 0.95 ± 0.03, twelve hours: 0.85 ± 0.04, 24 hours: 0.67 ± 0.05 μm/second). The distance traveled in each movement (Figure 6F) decreased in a similar fashion (baseline: 4.6 ± 1.1, six hours: 5.0 ± 1.2, twelve hours: 3.6 ± 0.6, 24 hours: 1.4 ± 0.3 μm) ($p < 0.05$ at 24 hours).

4. Discussion

We have developed an *in vitro* model of BIPN using a rat DRG neuronal culture system. This represents the first *in vitro* system that has studied BIPN specifically in the cells (DRG neurons) most severely affected in this condition. Using this model system we demonstrate that bortezomib causes an axonopathy without cell death, which is associated with increased tubulin polymerization and impaired axonal transport. Furthermore, these toxic sequelae of bortezomib appear to be a class effect as we see similar effects with an unrelated proteasome-inhibitor, lactacystin.

Whole rodent models have been developed wherein bortezomib administration produces a peripheral neuropathy, which in different studies have shown pathology to reside in the DRG (Carozzi et al., 2010), large myelinated axons (Bruna et al., 2010), small unmyelinated axons (Bruna, Udina, 2010, Carozzi, Canta, 2010, Meregalli et al., 2010), axonal

mitochondria (Zheng et al., 2012), or Schwann cells (Cavaletti et al., 2007, Shin et al., 2010). Although these studies have demonstrated BIPN in a model system, most of these studies have not explored mechanistically the reason for the development of neuropathy. Arastu-Kapur et al. (Arastu-Kapur et al., 2011) demonstrated disruption of neurites in a neuroblastoma cell line treated with bortezomib. They argued for proteasome-independent neuronal damage by bortezomib since they did not observe similar neurite damage with another proteasome inhibitor, carfilzomib; however, they did not use lactacystin as described in our study. Our data in rat DRG are in line with data by Poruchynsky et al., who used a variety of neuronal and non-neuronal *in vitro* cell lines (Sy5Y, KCNR, HCN2 and 8226) to demonstrate increased microtubule stabilization due to bortezomib.

An interesting finding in our study is that bortezomib increases microtubule polymerization, yet does not cause increased tubulin acetylation. While polymerization and acetylation are separate processes, they usually are found together. We hypothesize that both microtubule polymerization and acetylation must be regulated differentially by proteins that are separately influenced by proteasome degradation. Furthermore, there is likely a change in the distribution of tubulin and microtubules. With immunofluorescence, we observed sub-plasma membrane staining of tubulin without accompanying polymerized microtubules present electron microscopy. We interpret that this sub-plasma membrane tubulin immunofluorescence represents a redistribution of soluble tubulin monomers. It will be important to tease out the causes of tubulin polymerization and localization and how this may relate to the dysfunctional axonal transport observed.

Our data provide further evidence for the importance of axonal transport function in many forms of neurotoxicity (Staff et al., 2011). It is likely that neurons, with their metabolically-active long neuritic processes are preferentially susceptible to insults to axonal transport dysfunction. Abnormal mitochondrial dynamics have been implicated in progression of multiple neurodegenerative diseases (Su et al., 2010). For example, changes in mitochondrial distribution and axonal transport were affected in progression of Alzheimer's Disease (AD) under conditions that no cell death occurs (Wang et al., 2009, Wang et al., 2008), suggesting that abnormal mitochondrial dynamics may play important roles at early stages during the pathogenesis of AD (Trushina et al., 2012). These findings raise the possibility that strategies to improve axonal transport function may be useful in a number of neurological diseases as disparate as AD and chemotherapy-induced peripheral neuropathy.

Our *in vitro* studies demonstrating axonal dysfunction draw a strong parallel with the clinical phenotype of BIPN in humans. BIPN in human patients is characterized as a painful sensory neuropathy, with reduced amplitude sural sensory nerve action potentials and reversibility, which support a sensory axonopathy versus a neuronopathy. Our *in vitro* model using DRG neurons with widely arborizing axons provides an opportunity to specifically study the mechanisms of bortezomib axonal toxicity. This model revealed bortezomib-related changes that localized to the axons (axonal transport) that would not have been revealed in a non-neuronal system. The primary limitation of our *in vitro* DRG culture system is that it lacks the support cells (schwann cells, fibroblasts, etc.) present in an *in vivo* system that likely influence the cellular responses to toxic stress. Some researchers have further advocated studying BIPN using *in vivo* animal models bearing cancers, arguing that the presence of a cancer can further affect toxic effects of chemotherapy (Ceresa et al., 2011). We do feel that the *in vitro* embryonic rat DRG model system reported here will be useful to investigate BIPN further, understanding that there are limitations with any model system of human disease.

This study sets the foundation for further investigations into the mechanisms of BIPN. A key question regarding bortezomib's effects on DRG neurons is to determine disruption of

which part of the axonal transport system is the key mediator of the neurotoxicity. We have demonstrated that bortezomib disrupts multiple sites of the axonal transport system, including the microtubule tracks, the cargo (mitochondria), and possibly the energy supply (via disrupted mitochondrial localization), but our studies have not provided the temporal resolution to determine which is effected first (or if there is an upstream mediator of this effect). Future ongoing studies aim to investigate this issue in greater detail, which will be necessary in order to provide therapeutic targets to prevent BIPN.

Acknowledgments

This work was supported by NIH – (K08)CA169443 (NPS), NIH-NS40471 (AJW), NIH-ES20715 (ET), NIH – (T32)N5000794 (MB) and NIH-CA124477 (CLL). The authors wish to thank Scott Gamb for his technical assistance with electron microscopy and Kyle Howell for his technical assistance with Western blot analyses.

References

Adams J, Behnke M, Chen S, Cruickshank AA, Dick LR, Grenier L, et al. Potent and selective inhibitors of the proteasome: dipeptidyl boronic acids. Bioorganic & medicinal chemistry letters. 1998; 8:333–338. [PubMed: 9871680]

Arastu-Kapur S, Anderl JL, Kraus M, Parlati F, Shenk KD, Lee SJ, et al. Nonproteasomal targets of the proteasome inhibitors bortezomib and carfilzomib: a link to clinical adverse events. Clinical cancer research: an official journal of the American Association for Cancer Research. 2011; 17:2734–2743. [PubMed: 21364033]

Barr PM, Fu P, Lazarus HM, Horvath N, Gerson SL, Koc ON, et al. Phase I trial of fludarabine, bortezomib and rituximab for relapsed and refractory indolent and mantle cell non-Hodgkin lymphoma. Br J Haematol. 2009; 147:89–96. [PubMed: 19656151]

Boyette-Davis JA, Cata JP, Zhang H, Driver LC, Wendelschafer-Crabb G, Kennedy WR, et al. Follow-up psychophysical studies in bortezomib-related chemoneuropathy patients. J Pain. 2011; 12:1017–1024. [PubMed: 21703938]

Bross PF, Kane R, Farrell AT, Abraham S, Benson K, Brower ME, et al. Approval summary for bortezomib for injection in the treatment of multiple myeloma. Clin Cancer Res. 2004; 10:3954–3964. [PubMed: 15217925]

Bruna J, Udina E, Ale A, Vilches JJ, Vynckier A, Monbaliu J, et al. Neurophysiological, histological and immunohistochemical characterization of bortezomib-induced neuropathy in mice. Exp Neurol. 2010; 223:599–608. [PubMed: 20188093]

Carozzi VA, Canta A, Oggioni N, Sala B, Chiorazzi A, Meregalli C, et al. Neurophysiological and neuropathological characterization of new murine models of chemotherapy-induced chronic peripheral neuropathies. Exp Neurol. 2010

Cavaletti G, Gilardini A, Canta A, Rigamonti L, Rodriguez-Menendez V, Ceresa C, et al. Bortezomib-induced peripheral neurotoxicity: a neurophysiological and pathological study in the rat. Exp Neurol. 2007; 204:317–325. [PubMed: 17214983]

Ceresa, C.; Meregalli, C.; Bossi, M.; Pisano, C.; Vasci, L.; Fodera, R., et al. Neurophysiological and neuropathological evaluation of the bortezomib effect in myeloma-bearing mice. In: Wiley-Blackwell, editor. Journal of the Peripheral Nervous System; Meeting of the Peripheral Nerve Society; Potomac, Maryland. 2011. p. S19

Gill JS, Windebank AJ. Cisplatin-induced apoptosis in rat dorsal root ganglion neurons is associated with attempted entry into the cell cycle. The Journal of clinical investigation. 1998; 101:2842–2850. [PubMed: 9637718]

Lapointe NE, Morfini G, Brady ST, Feinstein SC, Wilson L, Jordan M. Effects of eribulin, vincristine, paclitaxel and ixabepilone on fast axonal transport and kinesin-1 driven microtubule gliding: Implications for chemotherapy-induced peripheral neuropathy. Neurotoxicology. 2013

Mauermann ML, Blumenreich MS, Dispenzieri A, Staff NP. A case of peripheral nerve microvasculitis associated with multiple myeloma and bortezomib treatment. Muscle Nerve. 2012; 46:970–977. [PubMed: 23225391]

Meregalli C, Canta A, Carozzi VA, Chiorazzi A, Oggioni N, Gilardini A, et al. Bortezomib-induced painful neuropathy in rats: a behavioral, neurophysiological and pathological study in rats. Eur J Pain. 2010; 14:343–350. [PubMed: 19695912]

Podratz JL, Knight AM, Ta LE, Staff NP, Gass JM, Genelin K, et al. Cisplatin induced Mitochondrial DNA damage in dorsal root ganglion neurons. Neurobiol Dis. 2011; 41:661–668. [PubMed: 21145397]

Poruchynsky MS, Sackett DL, Robey RW, Ward Y, Annunziata C, Fojo T. Proteasome inhibitors increase tubulin polymerization and stabilization in tissue culture cells: a possible mechanism contributing to peripheral neuropathy and cellular toxicity following proteasome inhibition. Cell Cycle. 2008; 7:940–949. [PubMed: 18414063]

Richardson PG, Briemberg H, Jagannath S, Wen PY, Barlogie B, Berenson J, et al. Frequency, characteristics, and reversibility of peripheral neuropathy during treatment of advanced multiple myeloma with bortezomib. J Clin Oncol. 2006; 24:3113–3120. [PubMed: 16754936]

Scuteri A, Nicolini G, Miloso M, Bossi M, Cavaletti G, Windebank AJ, et al. Paclitaxel toxicity in post-mitotic dorsal root ganglion (DRG) cells. Anticancer research. 2006; 26:1065–1070. [PubMed: 16619507]

Shin YK, Jang SY, Lee HK, Jung J, Suh DJ, Seo SY, et al. Pathological adaptive responses of Schwann cells to endoplasmic reticulum stress in bortezomib-induced peripheral neuropathy. Glia. 2010

Staff NP, Benarroch EE, Klein CJ. Neuronal intracellular transport and neurodegenerative disease. Neurology. 2011; 76:1015–1020. [PubMed: 21403113]

Su B, Wang X, Zheng L, Perry G, Smith MA, Zhu X. Abnormal mitochondrial dynamics and neurodegenerative diseases. Biochimica et biophysica acta. 2010; 1802:135–142. [PubMed: 19799998]

Ta LE, Espeset L, Podratz J, Windebank AJ. Neurotoxicity of oxaliplatin and cisplatin for dorsal root ganglion neurons correlates with platinum-DNA binding. Neurotoxicology. 2006; 27:992–1002. [PubMed: 16797073]

Traenckner EB, Wilk S, Baeuerle PA. A proteasome inhibitor prevents activation of NF-kappa B and stabilizes a newly phosphorylated form of I kappa B-alpha that is still bound to NF-kappa B. Embo J. 1994a; 13:5433–5441. [PubMed: 7957109]

Traenckner EB, Wilk S, Baeuerle PA. A proteasome inhibitor prevents activation of NF-kappa B and stabilizes a newly phosphorylated form of I kappa B-alpha that is still bound to NF-kappa B. The EMBO journal. 1994b; 13:5433–5441. [PubMed: 7957109]

Trushina E, Dyer RB, Badger JD 2nd, Ure D, Eide L, Tran DD, et al. Mutant huntingtin impairs axonal trafficking in mammalian neurons in vivo and in vitro. Mol Cell Biol. 2004; 24:8195–8209. [PubMed: 15340079]

Trushina E, Nemutlu E, Zhang S, Christensen T, Camp J, Mesa J, et al. Defects in mitochondrial dynamics and metabolomic signatures of evolving energetic stress in mouse models of familial Alzheimer's disease. PLoS One. 2012; 7:e32737. [PubMed: 22393443]

Voorhees PM, Orlowski RZ. The proteasome and proteasome inhibitors in cancer therapy. Annu Rev Pharmacol Toxicol. 2006; 46:189–213. [PubMed: 16402903]

Wang X, Su B, Lee HG, Li X, Perry G, Smith MA, et al. Impaired balance of mitochondrial fission and fusion in Alzheimer's disease. The Journal of neuroscience: the official journal of the Society for Neuroscience. 2009; 29:9090–9103. [PubMed: 19605646]

Wang X, Su B, Siedlak SL, Moreira PI, Fujioka H, Wang Y, et al. Amyloid-beta overproduction causes abnormal mitochondrial dynamics via differential modulation of mitochondrial fission/fusion proteins. Proc Natl Acad Sci U S A. 2008; 105:19318–19323. [PubMed: 19050078]

Windebank AJ, Smith AG, Russell JW. The effect of nerve growth factor, ciliary neurotrophic factor, and ACTH analogs on cisplatin neurotoxicity in vitro. Neurology. 1994; 44:488–494. [PubMed: 8145920]

Zheng H, Xiao WH, Bennett GJ. Mitotoxicity and bortezomib-induced chronic painful peripheral neuropathy. Exp Neurol. 2012; 238:225–234. [PubMed: 22947198]

- We develop an *in vitro* model of bortezomib-induced neuropathy using rat dorsal root ganglia.
- Bortezomib causes a sensory axonopathy based on whole explant outgrowth and cell survival assays
- Bortezomib causes accumulation of somatic tubulin and increased tubulin polymerization
- Bortezomib inhibits axonal transport of mitochondria

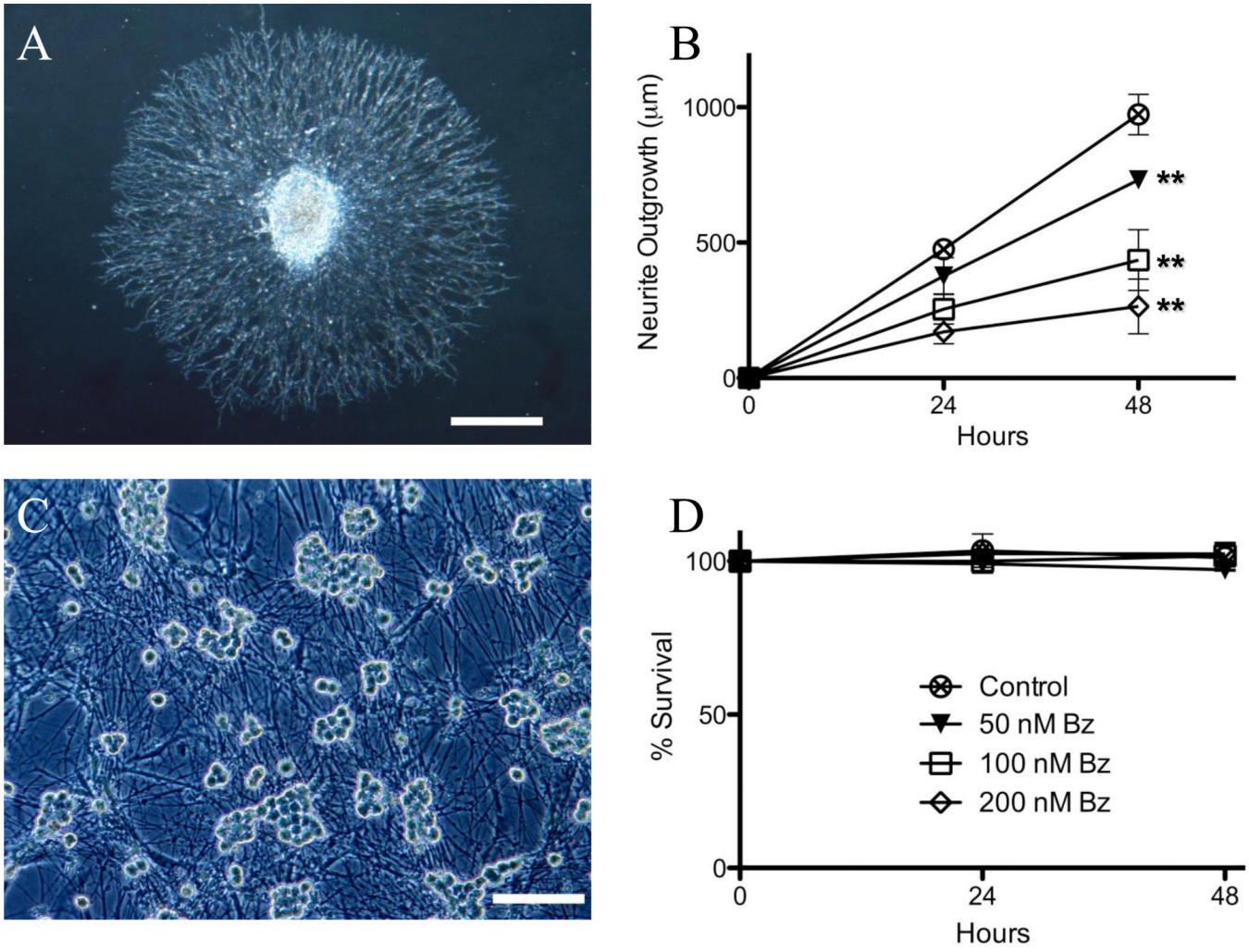

Figure 1. Bortezomib induces a concentration-dependent reduction in DRG neurite outgrowth without concomitant neuronal death

Rat E15 DRG neurite outgrowth is inhibited by bortezomib in a dose-dependent fashion (B); with an example of DRG neurite outgrowth explant culture (A, scale bar 100 μm). Dissociated DRG neuronal cultures do not exhibit cell death in the presence of bortezomib at varying concentrations (D), with an example of dissociated DRG neuronal cultures (C, scale bar 200 μm) (** – $p<0.05$).

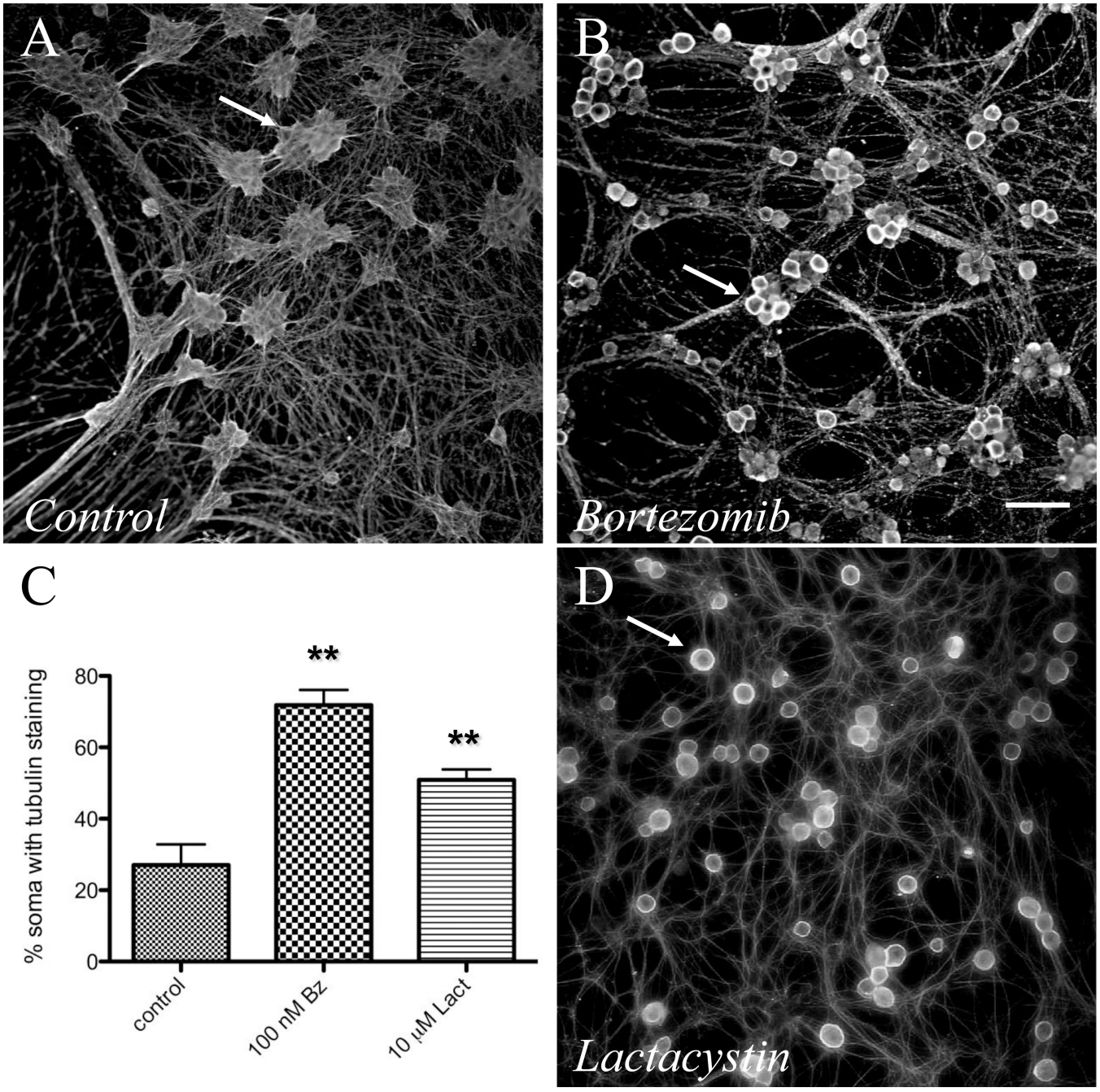

Figure 2. Bortezomib induces somatic aggregation of beta-tubulin

Low resolution epifluorescence (scale bar – 50 μm) images of dissociated DRG neuronal cultures. DRG neurons exposed to (B) bortezomib (100 nM) or (D) lactacystin (10 μM) exhibit somatic aggregation of beta-tubulin as determined by immunohistochemistry compared with controls (A). Arrows denote somata that show ring-like intense staining with bortezomib exposure. Increased numbers of somata exhibited tubulin aggregation in bortezomib (100 nM) and lactacystin (10 μM) treated dissociated DRG neuronal cultures (C, ** – $p<0.05$).

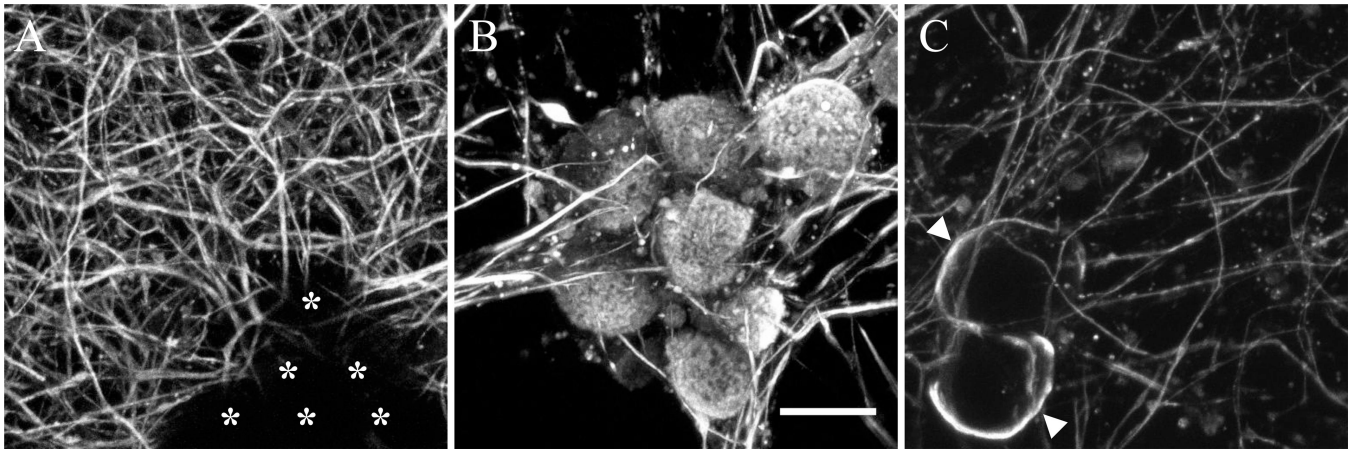

Figure 3. Sub-plasma membrane localization of tubulin aggregation

High resolution laser scanning confocal microscopy images compressed into z-stacks (scale bar – 20 μm) for control (A) and bortezomib 100 nM exposure (B, C) stained for beta-tubulin. Note the somatic staining in bortezomib that is lacking in control conditions (asterisks show cell bodies). A single z-plane (C) illustrates the sub-plasma membrane localization of tubulin staining (arrowheads).

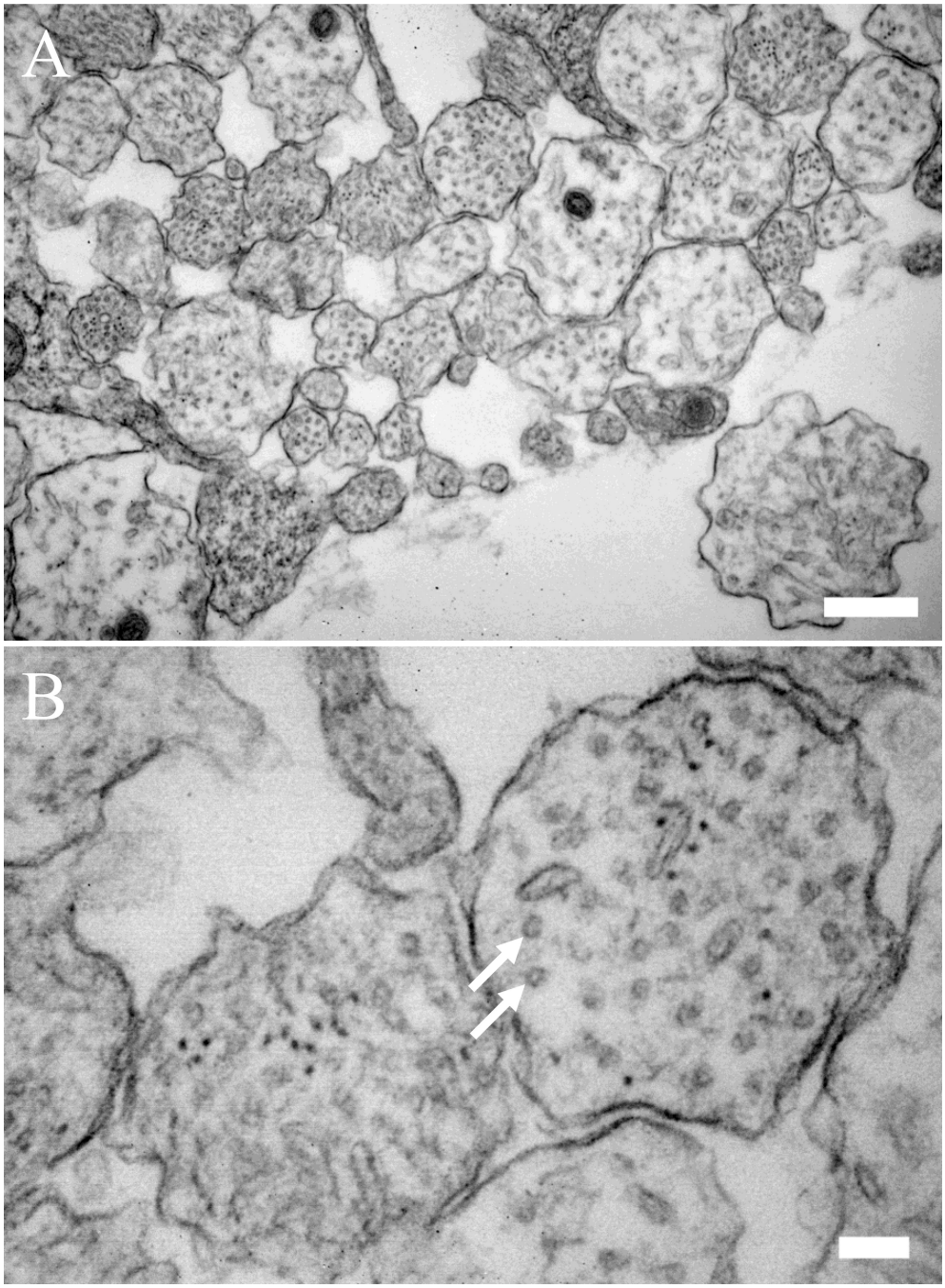

Figure 4. Bortezomib does not alter microtubule ultrastructure

Transmission electron micrographs of DRG explant cultures exposed to bortezomib (100 nM) at low power (A – scale bar 500 nm) and high power (B – scale bar 100 nm). Microtubules in cross section are easily seen throughout (arrows).

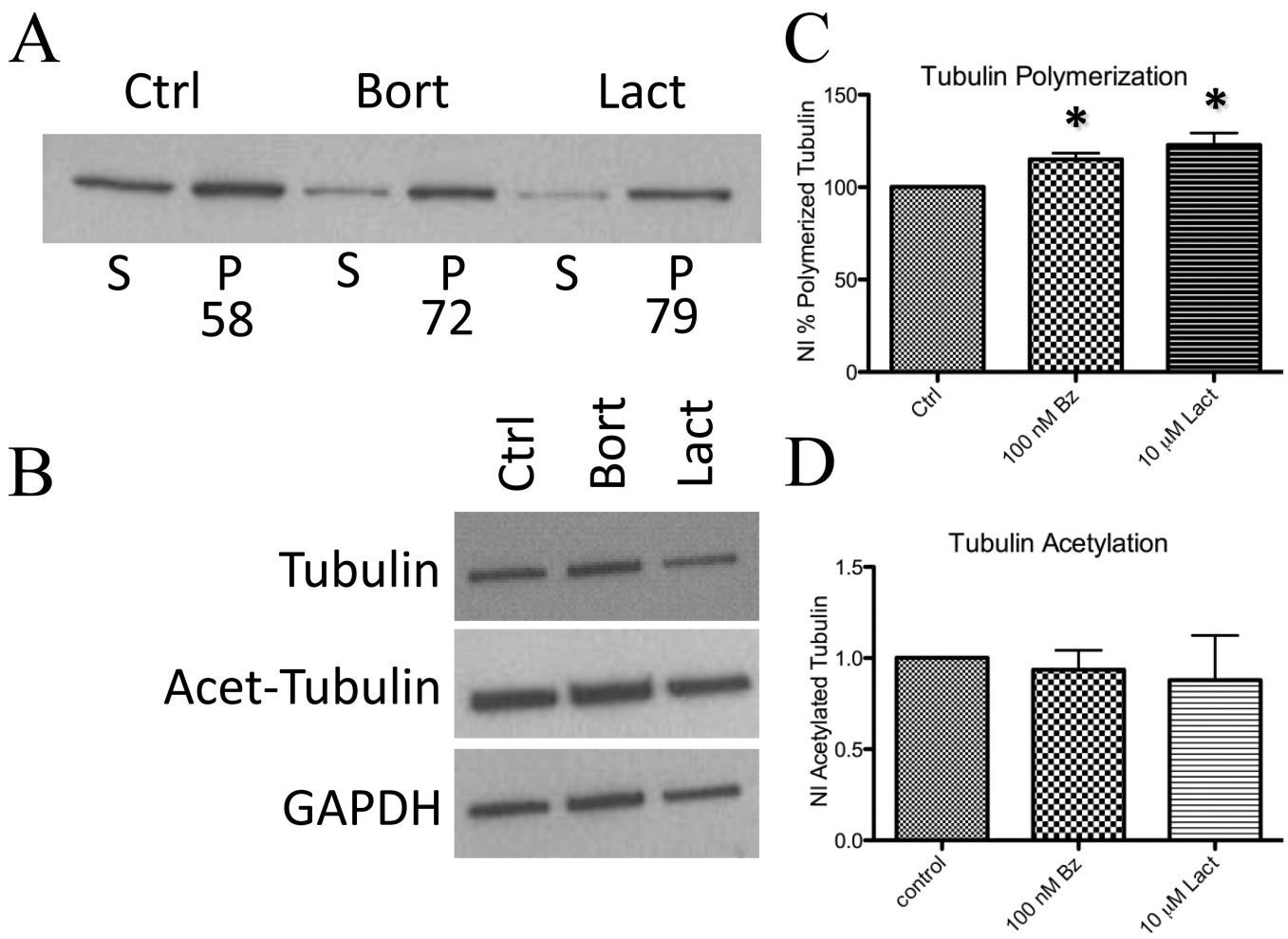

Figure 5. Bortezomib increases tubulin polymerization without an increase in tubulin acetylation

Western blot analysis of rat DRG neuronal cultures. Equal volumes of protein lysate demonstrate increased percentage of polymerized (P) versus soluble (S) tubulin (P / S + P) in rat DRG neurons treated for 24 hours with 100 nM bortezomib (Bort – 72%) and 10 uM lactacystin (Lact – 79%) or control (Ctrl – 58%) (A). Normalized percentages of polymerized tubulin are increased in both bortezomib and lactacystin (C – *- $p < 0.05$). There is no increased amount of acetylated tubulin after treatment of rat DRG neurons with bortezomib or lactacystin (B, D).

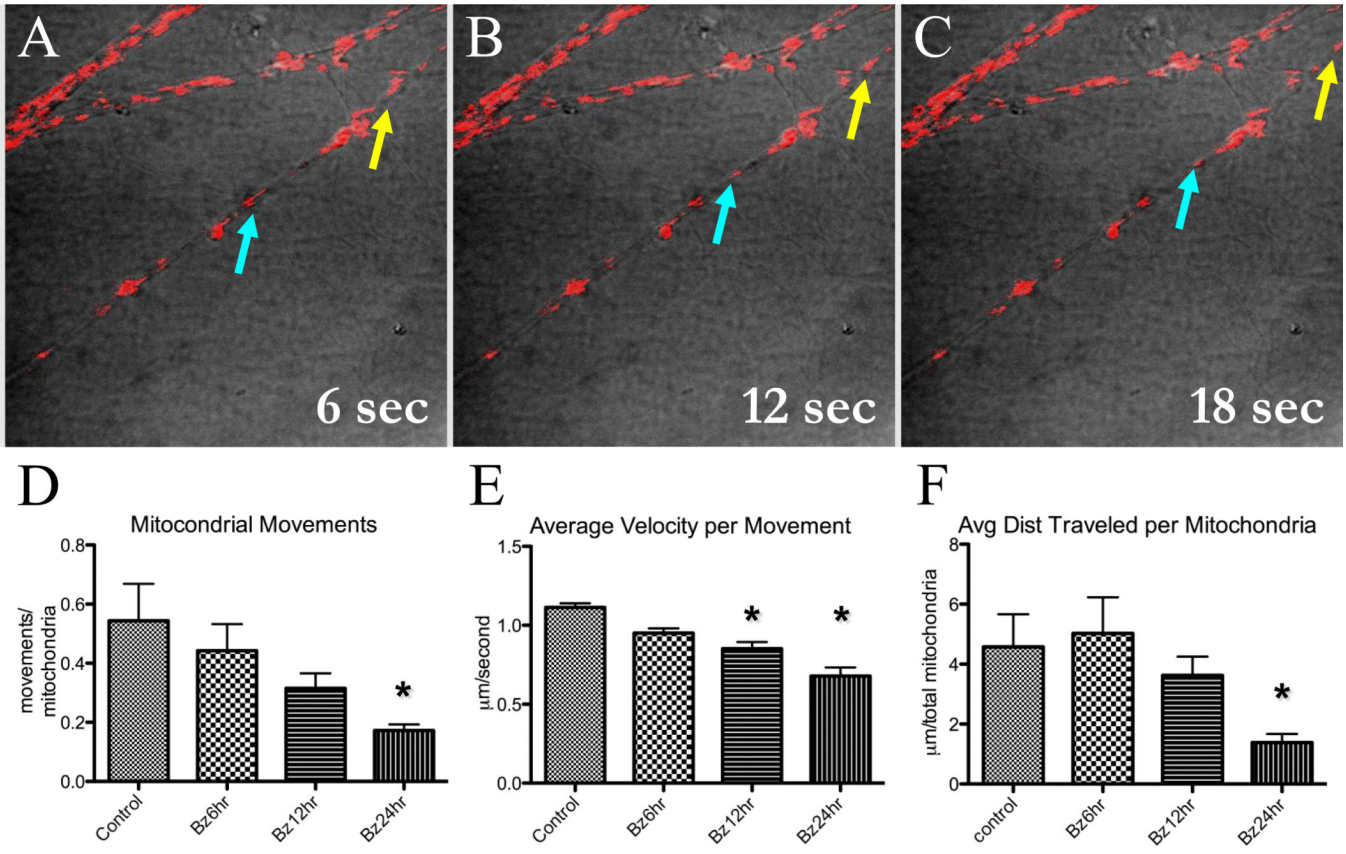

Figure 6. Axonal trafficking of mitochondria is inhibited in bortezomib-treated DRG neurons

Live imaging of mitochondria was performed using the mitochondrial label TMRM (10 nM) with cultures exposed to bortezomib (100 nM) at varying times. Five minute movies were performed with a single confocal image acquisition per second and subsequently analyzed off-line. Still frames from the movies are denoted in A–C where motile mitochondria are easily recognized and analyzed (blue and yellow arrows track two motile mitochondria). The total numbers of mitochondria analyzed for all conditions were not significantly different. With increasing exposure time to bortezomib treatment, there was a decrease in numbers of movements (D), average velocity (E), and distance traveled (F) per mitochondria. (* –, $p < 0.05$).